J Mater Sci: Mater Electron (2024) 35:1243

A.C. Permittivity and conductivity studies of Ni-doped Pb levo-tartrate crystals

N. D. Pandya[1,*], J. H. Joshi[2], D. J. Dave[1], R. R. Hajiyani[3], H. O. Jethva[4], and M. J. Joshi[1]

[1] *Department of Physics, Faculty of Science, Atmiya University, Rajkot 360005, Gujarat, India*
[2] *Regional Forensic Science Laboratory, Physics Division, Rajkot 360005, Gujarat, India*
[3] *Forensic Science Laboratory, Gandhinagar 382021, Gujarat, India*
[4] *Crystal Growth Laboratory, Department of Physics, Saurashtra University, Rajkot 360005, Gujarat, India*

Received: 30 November 2023
Accepted: 7 June 2024

ABSTRACT

Lead Tartrate finds several applications such as an additive in gasoline to prevent knocking in motors, in synthesis of chiral molecules, and a combustion catalyst in solid propellant. To modify the properties of PbLT (lead levo-tartrate), the Ni addition is done. The lead nitrate and nickel nitrate solutions are used to grow Pb–Ni levo-tartrate (PbNiLT) crystals in silica gel medium. The amount of Ni and Pb is determined by EDAX. Powder XRD reveals the outcome of Ni addition on the lattice constants of PbLT crystals. The presence of certain functional groups is noticed by FTIR spectra. TGA suggests that Ni increases the thermal stability of PbNiLT crystals compared to PbLT crystals. The A.C. electrical characteristics of PbLT and PbNiLT such as dielectric, impedance, and modulus spectroscopy are studied. This reveals microstructural effect by adding Ni in PbLT crystals, and from the complex impedance Nyquist plots, the grain resistance R_g, grain capacitance C_g, and relaxation frequency values are obtained along with fitting with equivalent R–C circuit. The behavior of relaxation mechanism prevailing in the PbLT and PbNiLT crystals is explained.

1 Introduction

Lead Tartrate (PbLT) is known as knocking prevention agent in motors operated by gasoline [1], as a precursor for yielding chiral molecular magnets [2] and a combustion catalyst in solid propellant [3]. The gel growth technique has attracted attention of large number of researchers for crystals which are very less soluble in water and decompose on heating [4, 5]. The gel growth of lead (Pb) levo-tartrate (PbLT) crystals was reported [6]. The literature survey reveals elaborative exploration of structural [7], spectroscopic [7], morphological studies [8], thermal studies [9], and impedance and modulus spectral studies of pure Pb LT. Lead tartrate showed the dendritic growth in gel media, which is well explained in the literature by some authors [7, 9]. Similarly, growth of pure nickel tartrate crystals in gel medium and its EDAX, SEM, XRD, and FTIR study has been reported [10]. Further, some nickel-doped tartrate crystals and their characterization have also been reported [11–14]. Apart from these, ternary levo-tartrate

Address correspondence to E-mail: nikunj.pandya@atmiyauni.ac.in; pandyanikunj19@gmail.com

https://doi.org/10.1007/s10854-024-12940-7
Published online: 25 June 2024

crystals of iron-manganese-nickel are also reported [11]. Nickel tartrate finds application as a catalyst in hydrogenation process [15] and food industry and pharmaceutical industry [16].

Above survey reveals that, very limited reports are available on A.C. electrical studies of PbLT. To modify the properties of PbLT crystal, the nickel doping is selected as it belongs to 3d transition element having more than one valency with smaller atomic/ionic radius and finding applications in industry as mentioned above. Therefore, authors are tempted to carry out A.C. electrical studies including impedance and modulus spectroscopic studies of pure and Ni-added PbLT along supplementary studies such as X Ray Diffraction, FTIR, EDAX, and Thermo gravimetric analysis. The novelty of the work is that the detailed impedance and modulus studies are carried out as these properties are helpful to define possible electrical application.

2 Experimental details

The single diffusion gel growth technique was implemented to grow pure Pb and Ni-added Pb LT crystals which is explained in Fig. 1. As a growth medium of the above-mentioned crystals, congealed gel of SMS is employed. The supernatant solutions of compositions mentioned in Table 1 were poured gently over the surface of set gel without disturbing gel structure.

L-tartaric acid is used to acidify gel. The diffusion of Pb^{2+} and Ni^{2+} in the set gel reacts with tartrate ions present in gel matrix. The expected chemical reaction is expressed as below:

$$(1-X)Pb(NO_3)_2 \cdot 6H_2O(aq) + XNi(NO_3)_2 \cdot 6H_2O(aq) + H_2C_4H_4O_6 + nH2O \rightarrow NiXPb(1-X)C_4H_4O_6nH_2O + 4HNO_3 + 11H_2O + O_2$$

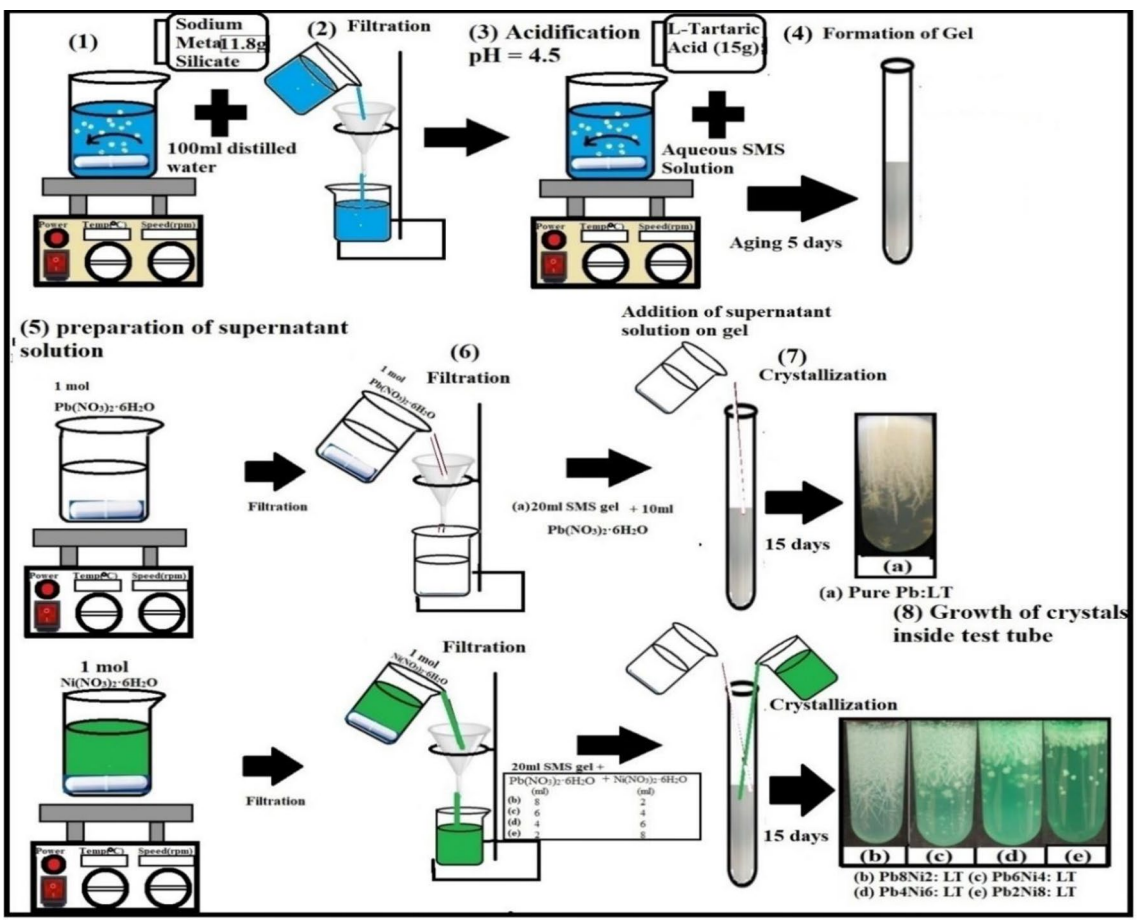

Fig. 1 Experimental Technique

Table 1 Volume compositions of supernatant solution

Sample code	Sample name LT is levo-tartrate	Name of supernatant solution			
		$Pb(NO_3)_2{\cdot}6H_2O$		$Ni(NO_3)_2{\cdot}6H_2O$	
		Volume (ml)	Mol	Volume (ml)	Mol
(a)	Pure Pb: LT	10	1	00	1
(b)	Pb8Ni2: LT	08	1	02	1
(c)	Pb6Ni4:LT	06	1	04	1
(d)	Pb4Ni6:LT	04	1	06	1
(e)	Pb2Ni8:LT	02	1	08	1

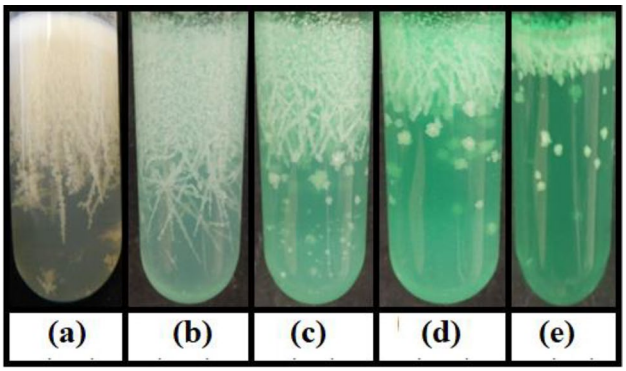

Fig. 2 Growth of **a** Pure Pb:LT **b** Pb8Ni2:LT **c** Pb6Ni4:LT **d** Pb4Ni6:LT and **e** Pb2Ni8:LT crystals inside test tubes

To vary concentration of Ni in Pb LT, the values of X = 0.0, 0.2, 0.4, 0.6, and 0.8 are adjusted depending on the addition of $Ni(NO_3)_2{\cdot}6H_2O$ solution. However, the exact content and stoichiometry of crystals are determined from EDAX analysis.

Figure 2 depicts photographs of grown crystals.

Figure 2 shows that increase in concentration of Pb^{2+} ions promotes dendrite morphology [Fig. 2e–a], whereas increase in concentration of Ni^{2+} promotes spherulitic morphology and color variation from whitish to greenish [Fig. 2a–e].

3 Characterization of crystals

3.1 Energy-dispersive X-ray analysis (EDAX)

To determine concentration of Ni^{2+} and Pb^{2+} in Ni added PbLT crystals, energy-dispersive X-ray analysis (EDAX) technique was employed.

The EDAX spectra of pure and Ni-added Pb LT crystals are shown in Fig. 3.

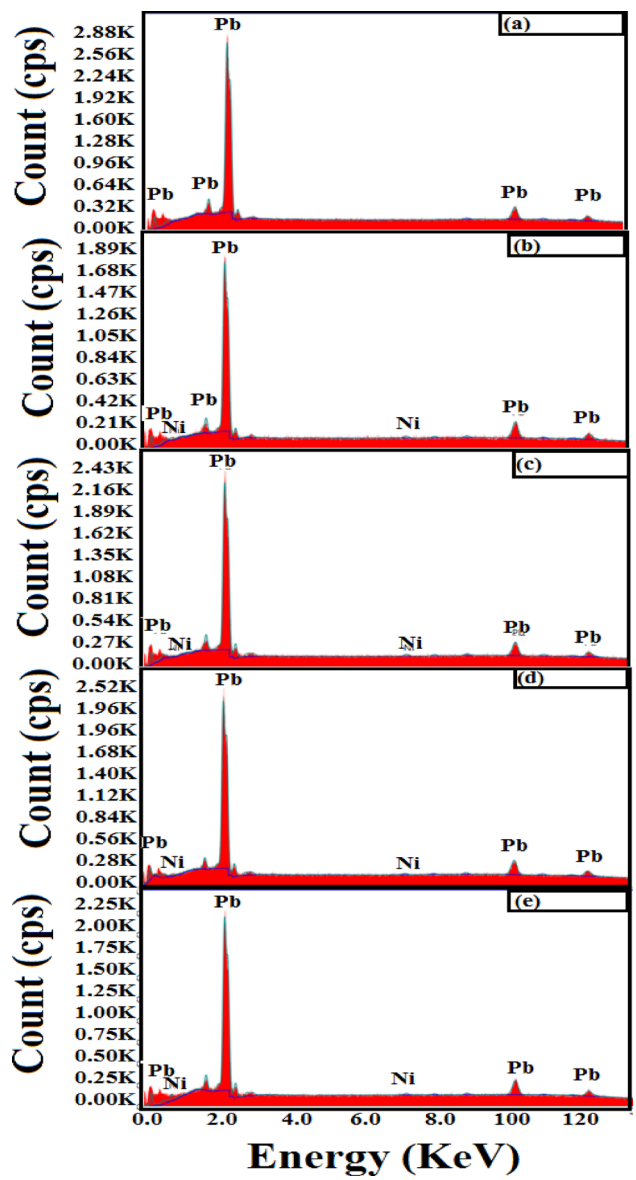

Fig. 3 The EDAX spectrum of **a** Pure Pb:LT **b** Pb8Ni2:LT **c** Pb6Ni4:LT **d** Pb4Ni6:LT and **e**Pb2Ni8:LT

Table 2 Expected and observed (From EDAX) atomic weight% values of lead as well as nickel in the grown crystals

Sample no	Proposed formula	Expected Atomic weight (%)		From EDAX Atomic weight (%)	
		Element		Element	
		Pb	Ni	Pb	Ni
1	$PbC_4H_4O_6{\bullet}nH_2O$	100	0	–	–
2	$Pb_{0.8}Ni_{0.2}C_4H_4O_6{\bullet}nH_2O$	80	20	98.93	1.07
3	$Pb_{0.6}Ni_{0.4}C_4H_4O_6{\bullet}nH_2O$	60	40	98.23	1.77
4	$Pb_{0.4}Ni_{0.6}C_4H_4O_6{\bullet}nH_2O$	40	60	97.86	2.14
5	$Pb_{0.2}Ni_{0.8}C_4H_4O_6{\bullet}nH_2O$	20	80	97.73	2.27

Table 3 Estimated molecular formula from EDAX

Sample code	Estimated formula by EDAX
(a) Pure Pb:LT	$PbC_4H_4O_6{\bullet}nH_2O$
(b) Pb8Ni2:LT	$Pb_{0.989}Ni_{0.011}C_4H_4O_6{\bullet}nH_2O$
(c) Pb6Ni4:LT	$Pb_{0.982}Ni_{0.018}C_4H_4O_6{\bullet}nH_2O$
(d) Pb4Ni6:LT	$Pb_{0.979}Ni_{0.021}C_4H_4O_6{\bullet}nH_2O$
(e) Pb2Ni8:LT	$Pb_{0.977}Ni_{0.023}C_4H_4O_6{\bullet}nH_2O$

Expected and observed atomic Wt% values of lead and nickel and proposed formula are given in Table 2, while the estimated formula for the relevant crystals is given in Table 3.

Table 2 indicates the trend of variation in atomic weight percentages of Pb^{2+} and Ni^{2+} in Pb LT as per the increase or decrease in volume concentrations of lead nitrate and nickel nitrate hexahydrate solutions in supernatant solutions poured on set gels. The experimental data of the atomic weight percentages of Pb^{2+} and Ni^{2+} in the harvested crystals do not match with expected one. All these crystals contain major atomic weight % of Pb^{2+} ions compared to Ni^{2+} ions which is due to vast difference in hydrated radii of Pb^{2+} and Ni^{2+} ions. Being a smaller ion and having greater ionic potential attract more water molecules, the thickness of hydration shell, i.e., layer of water molecules of Ni^{2+} is greater than that of Pb^{2+} ion. The inverse relationship is observed between non-hydrated radius and hydrated radius of Pb^{2+} and Ni^{2+} ion. In this study, the non-hydrated radius of Pb^{+2} is 1.19 Å and second ionization potential is 15.028 eV, while the same quantities for Ni^{+2} are 0.69 Å and 18.168 eV, respectively [17]. Therefore, the reverse nature is observed for hydrated radii of Pb^{+2} and Ni^{+2} than that for the non-hydrated ones [18, 19].

The molecular formulae for grown crystals are used as per given in Table 3.

3.2 Powder XRD analysis

The powder X-ray diffraction patterns of Pb LT and nickel-added Pb LT crystals are depicted in Fig. 4a–e. The evaluated unit cell parameters are listed in Table 4.

As the apparent Wt% of Ni^{2+} is very less in Ni-added Pb LT crystals, all the XRD patterns of Ni-added Pb LT show change in peak intensity along with minor peak shifting which confirms the presence of Ni in Pb LT crystals. Hence, the estimated lattice parameters of Ni-added Pb LT are found nearby that of Pb LT. The overlapping of XRD patterns indicates that Ni-added Pb LT exhibits single phase nature.

As the heavier atom like Pb is more capable for effective scattering of X rays compared to lighter one like Ni, the enhanced peak intensity of a particular plane is due to the presence of Pb in that plane. However, the reduction in peak intensity of particular plane is due to the existence of Ni in that plane. This type of peak intensity changes reflects that the distribution of Pb and Ni atoms in particular plane influence the total scattering occurring. That means a change in peak intensity is correlated to the difference of total scattering taking place from each crystalline planes due to distribution of lead and nickel atoms in the crystalline structure, which in turn, is related with composition of prepared the samples. Further, the separate peaks of nickel are not identified in Ni-added PbLT crystals as the Wt% of Ni in PbLT crystals is meager. Further, the Ni addition in Pb LT causes shifting of peaks toward lower 2θ value, indicating expansion in the unit cell volume and lattice parameters.

To determine lattice strain and average crystallite size of PbLT and PbNiLT, the Williamson-Hall (W-H) method [20] is applied.

Table 5 indicates the presence of minimum lattice strain for PbLT, suggesting the minimum distortion in grain, density of point defects, and residual stresses. The strain values increase gradually due to the increase of Ni content in PbLT crystals. The increment in lattice strain is because of the difference between Ionic radii of Pb (1.19 Å) and Ni (0.69 Å). That means that the lattice strain and distortion of crystal lattice are promoted by cationic substitution of larger

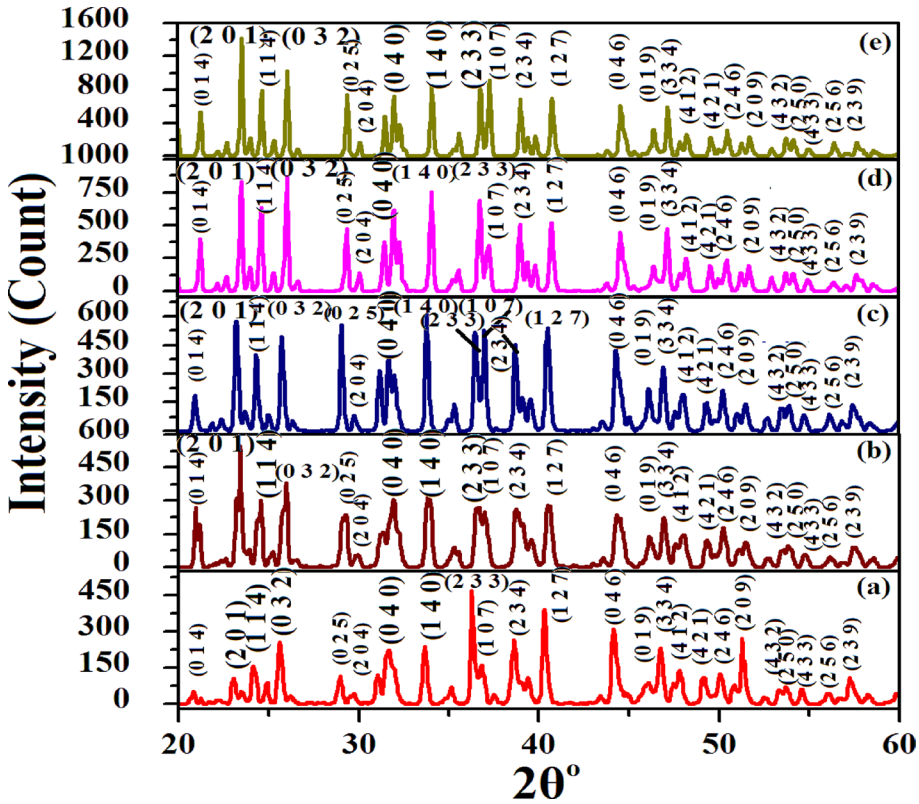

Fig. 4 Powder XRD pattern of **a** Pure Pb:LT **b** Pb8Ni2:LT **c** Pb6Ni4:LT **d** Pb4Ni6:LT and **e**Pb2Ni8:LT

Table 4 Lattice parameters and crystal system of grown crystals

Sample code	Unit cell parameters and crystal system		
	Orthorhombic $\alpha=\beta=\gamma=90^o$		
	a(Å) ± 0.0635	b(Å) ± 0.113	c(Å) ± 0.158
(a) Pure Pb: LT	7.975	11.114	17.969 ± 0.158
(b) Pb8Ni2: LT	7.814	11.371	18.075 ± 0.158
(c) Pb6Ni4:LT	7.948	11.335	18.077 ± 0.158
(d) Pb4Ni6:LT	7.927	11.340	18.024 ± 0.158
(e) Pb2Ni8:LT	7.953	11.395	18.375 ± 0.158

Table 5 Estimated Strain values and crystallite size from W–H analysis of **a** Pure Pb:LT **b** Pb8Ni2:LT **c** Pb6Ni4:LT **d** Pb4Ni6:LT and **e**Pb2Ni8:LT

Sample code	Lattice strain (η) ± 0.0022	Average crystallite size nm) ± 15.73
(a) Pure Pb:LT	0.00347	36.2
(b) Pb_8Ni_2:LT	0.00576	45.9
(c) Pb_6Ni_4:LT	0.00610	50.7
(d) Pb_4Ni_6:LT	0.00829	70.0
(e) Pb_2Ni_8:LT	0.00895	72.6

cation, i.e., Pb, by smaller cation, i.e., Ni. The increased average crystallite size of Ni-added PbLT is also verified by the reduction in FWHM of peaks of Ni-added PbLT crystals.

3.3 FTIR spectroscopy study

The FTIR Spectra of PbLT and Ni-added PbLT, i.e., NiPbLT crystals, are depicted in Fig. 5. The characteristic absorption frequencies assigned to various functional groups and their various modes of vibrations [21–24] are categorized in Table 6.

As the apparent concentration of Ni in Ni-added PbLT crystals is very small, the characteristic absorption frequencies of functional groups are slightly changed. However, increase in Ni concentration in PbLT slightly alters metal–oxygen vibrations in low wave number region because of difference of atomic mass numbers, i.e., Pb (207amu) and Ni (58.69amu), and difference in ionic radii, i.e., Pb (1.19 Å) and Ni (0.69 Å).

The absorption frequency range for O–H stretching vibrations slightly varies in the range from 3383 to 3393 cm^{-1} due to minor concentration of Ni in PbLT which ultimately produces minor variation in stiffness

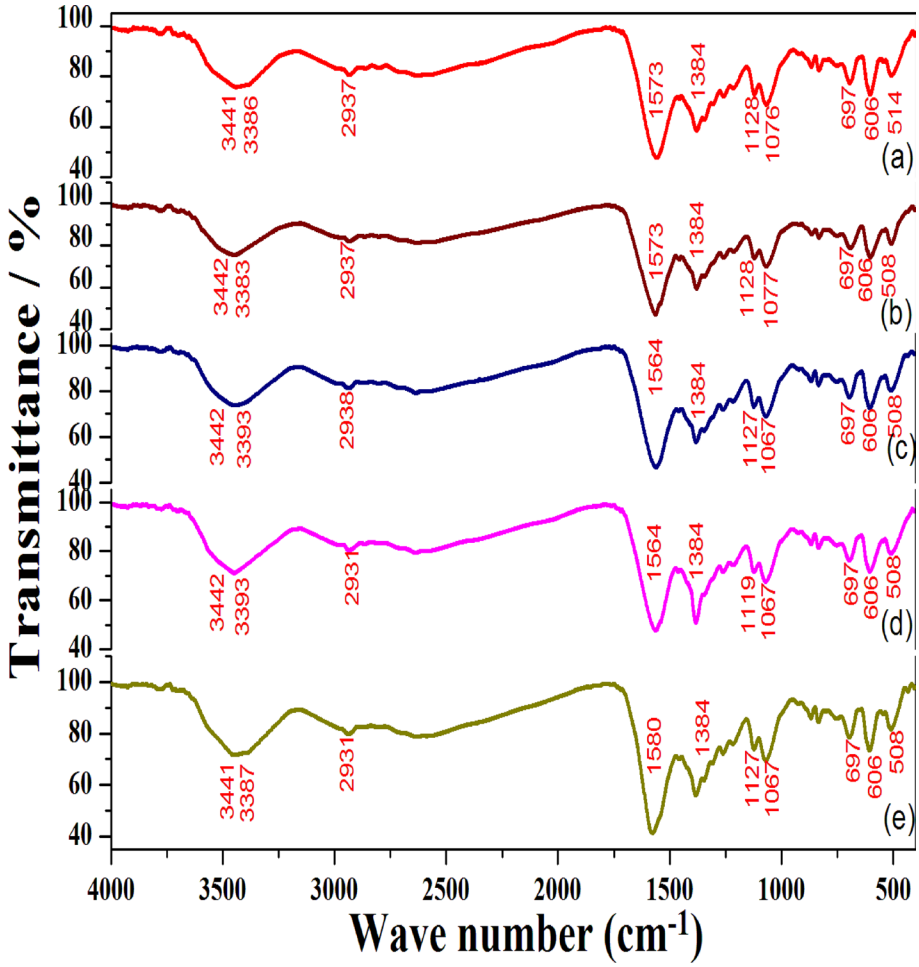

Fig. 5 FTIR spectra of **a** Pure Pb:LT **b** Pb8Ni2:LT **c** Pb6Ni4:LT **d** Pb4Ni6:LT and **e** Pb2Ni8:LT

Table 6 Functional groups with their characteristic absorption frequencies

Assignments	Wave number in cm^{-1} ±0.15				
	(a) Pure Pb: LT	(b) Pb8Ni2: LT	(c) Pb6Ni4: LT	(d) Pb4Ni6: LT	(e) Pb2Ni8: LT
O–H Stretching	3441 3386	3442 3383	3442 3393	3442 3393	3441 3387
Asymmetrical C–H Stretching	2937	2937	2938	2931	2931
C=O Stretching	1573	1573	1564	1564	1580
O–H bending In-plane or C–OH bending	1384	1384	1384	1384	1384
C–O Stretching	1128 1076	1128 1077	1127 1067	1119 1067	1127 1067
O–H bending out-of-plane, C–H deformation and C–H bending	697 606	697 606	697 606	697 606	697 606
Pb–O and Ni–O Stretching	514	508	508	508	508

Table 7 O–H bond force constant k for PbLT and PbNiLT crystals

Sample code	Force constant k in N/m ± 1.34
(a) Pure Pb: LT	644
(b) Pb8Ni2: LT	643
(c) Pb6Ni4:LT	646
(d) Pb4Ni6:LT	646
(e) Pb2Ni8:LT	644

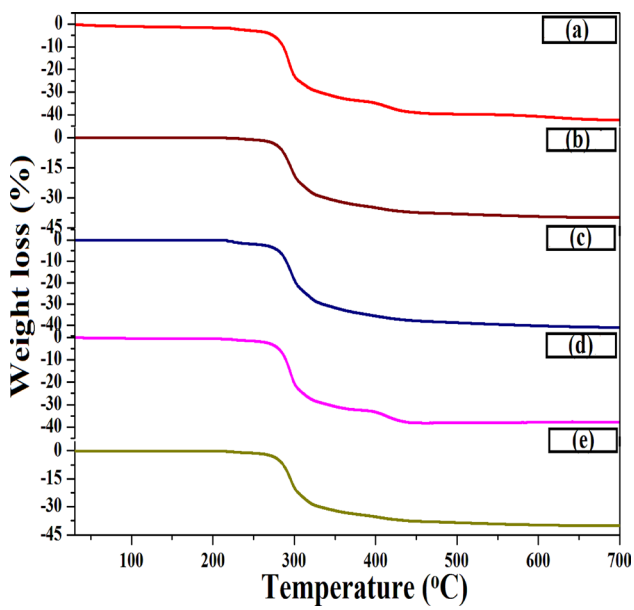

Fig. 6 Thermal decomposition profile of **a** Pure Pb:LT **b** Pb8Ni2:LT **c** Pb6Ni4:LT **d** Pb4Ni6:LT and **e** Pb2Ni8:LT

of the O–H bond and can be verified by calculation of force constant of O–H bond of the samples.

The force constant, k, of O–H bonding of pure PbLT and PbNiLT crystals is determined by the correlation between absorption frequency and force constant as already discussed in elaborative manner by Joshi and Joshi [25].

The force constant values for PbLT and PbNiLT crystals are compiled in Table 7. The values of k are slightly changed because of Ni addition in PbLT crystals.

3.4 Thermo gravimetric analysis (TGA)

The thermal decomposition profiles of PbLT and PbNiLT crystals are given in Fig. 6a–e. The identified decomposition stages and their temperature ranges are made available in Table 8.

From the comparison of thermal stabilities of Pb LT (215 °C) and PbNiLT (225 °C), the Ni addition induces increment in the thermal stability of PbLT. The TGA curves reveal three stage decomposition profile involving (1) dehydration stage, (2) carbonate stage, and (3) oxide stage of all crystals analyzed. For each decomposition stage, the corresponding mass losses values are given in percentage (%) in Table 8.

The correct stoichiometric formulae for the PbLT and PbNiLT crystals are available in Table 9 after the EDAX and TGA study, which will be used for the remaining discussion.

The plateaus on the TG profiles of Fig. 6 indicate the existence of stable stoichiometric compounds.

3.5 Dielectric constant (ε')

The changes occurring in dielectric constant (ε') with angular frequency of applied field are displayed in Fig. 7.

From the trend of variation of ε' curves, it is found that all the samples exhibit usual dielectric behavior [26] over the frequency range considered for PbLT and PbNiLT crystals.

3.6 Dielectric loss (ε'')

Figure 8 shows the trend of variation of dielectric loss (ε'') curves with respect to angular frequency for PbLT and PbNiLT samples. The ε'' curves are showing variation corresponding to dielectric constant curves. The high values of ε'' in low frequency regime are due to retention of space charge polarization.

The reduction of dielectric loss of Ni-added Pb LT crystals is because of the presence of nickel in the grain which favors the reduction grain capacitance and dielectric loss.

3.7 AC conductivity (σ_{ac})

Figure 9 shows the dependency of AC conductivity (σ_{ac}) on angular frequency at room temperature for PbLT and PbNiLT. The σ_{ac} curves for PbLT and PbNiLT samples are divided into two regions: (i) a low angular frequency flat or plateau region and (ii) a high frequency dispersion region.

The higher angular frequency regime indicates the frequency dependency of σ_{ac} and shows sharp increase

Table 8 Thermal decomposition stages with reaction involved

Sample code	Temperature interval (°C)	Expected reaction	Theoretically obtained mass loss in %	From TG plot obtained mass loss in %
(a) Pure Pb: LT	30–215	Almost Stable, No reaction	00	00
	215–275	$PbC_4H_4O_6{\cdot}H_2O \rightarrow PbC_4H_4O_6 + H_2O$	05.00	4.50
	275–330	$PbC_4H_4O_6 \rightarrow PbCO_3 + CH_4 + 2CO + 1/2O_2$	29.00	30.00
	330–650	$PbCO_3 \rightarrow PbO + CO_2$	40	41.00
(b) Pb8Ni2: LT	30–225	Stable, No reaction	00	00
	225–270	$Pb_{0.989}Ni_{0.011}C_4H_4O_6{\bullet}0.5H_2O \rightarrow Pb_{0.989}Ni_{0.011}C_4H_4O_6 + 0.5H_2O$	02.50	02.00
	270–320	$Pb_{0.989}Ni_{0.011}C_4H_4O_6 \rightarrow Pb_{0.989}Ni_{0.011}CO_3 + CH_4 + 2CO + 1/2O_2$	27.00	27.00
	320–600	$Pb_{0.989}Ni_{0.011}CO_3 \rightarrow Pb_{0.989}Ni_{0.011}O + CO_2$	39.00	39.6
(c) Pb6Ni4:LT	30–225	Stable, No reaction	00	00
	225–270	$Pb_{0.982}Ni_{0.018}C_4H_4O_6{\bullet}0.6H_2O \rightarrow Pb_{0.982}Ni_{0.018}C_4H_4O_6 + 0.6H_2O$	03.00	03.07
	270–320	$Pb_{0.982}Ni_{0.018}C_4H_4O_6 \rightarrow Pb_{0.982}Ni_{0.018}CO_3 + CH_4 + 2CO + 1/2O_2$	27.00	27.00
	320–700	$Pb_{0.982}Ni_{0.018}CO_3 \rightarrow Pb_{0.982}Ni_{0.018}O + CO_2$	44.00	39.4
(d) Pb4Ni6:LT	30–225	Stable, No reaction	00	00
	225–280	$Pb_{0.979}Ni_{0.021}C_4H_4O_6{\bullet}1.03H_2O \rightarrow Pb_{0.979}Ni_{0.021}C_4H_4O_6 + 1.03H_2O$	05.00	05.33
	280–330	$Pb_{0.979}Ni_{0.021}C_4H_4O_6 \rightarrow Pb_{0.979}Ni_{0.021}CO_3 + CH_4 + 2CO + 1/2O_2$	29.00	30.00
	330–700	$Pb_{0.979}Ni_{0.021}CO_3 \rightarrow Pb_{0.979}Ni_{0.021}O + CO_2$	40.00	41.00
(e) Pb2Ni8: LT	30–225	Stable, No reaction	00	00
	225–270	$Pb_{0.977}Ni_{0.023}C_4H_4O_6{\bullet}0.5H_2O \rightarrow Pb_{0.977}Ni_{0.023}C_4H_4O_6 + 0.5H_2O$	02.50	03.00
	270–320	$Pb_{0.977}Ni_{0.023}C_4H_4O_6 \rightarrow Pb_{0.977}Ni_{0.023}CO_3 + CH_4 + 2CO + 1/2O_2$	28.00	29.00
	320–600	$Pb_{0.977}Ni_{0.023}CO_3 \rightarrow Pb_{0.977}Ni_{0.023}O + CO_2$	40.00	39.80

Table 9 The correct stoichiometric formula

Sample code	The correct stoichiometric formula from TGA
(a) Pure Pb:LT	$PbC_4H_4O_6{\cdot}H_2O$
(b) Pb8Ni2:LT	$Pb_{0.989}Ni_{0.011}C_4H_4O_6{\bullet}0.5H_2O$
(c) Pb6Ni4:LT	$Pb_{0.982}Ni_{0.018}C_4H_4O_6{\bullet}0.6H_2O$
(d) Pb4Ni6:LT	$Pb_{0.979}Ni_{0.021}C_4H_4O_6{\bullet}1.03H_2O$
(e) Pb2Ni8:LT	$Pb_{0.977}Ni_{0.023}C_4H_4O_6{\bullet}0.5H_2O$

in σ_{ac} due to rise in frequency of applied field. The frequency which marks boundary between dispersion region and plateau region is defined as characteristic frequency (ω_p), also known as hopping rate.

3.8 Jonscher's plots

The Jonscher's power law explains the temperature and frequency dependency of electrical conductivity through a standard equation [27].

Figure 10 depicts Jonscher's plot for PbLT and PbNiLT and exhibits dispersive nature due to existence of AC conductivity in higher frequency part of dielectric spectrum. The values of Jonscher's parameters s and A are obtained from the slope and intercept of the Jonscher's plots and are given in Table 10.

The highest value of polarizability strength A is found for PbLT. The adding Ni in PbLT decreases its polarizability strength A. Now, due to direct relation between dielectric constant and polarizability

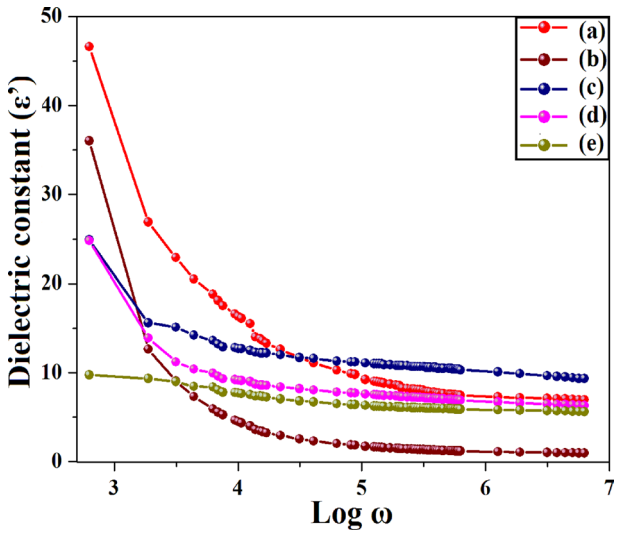

Fig. 7 Dielectric constant (ε′) curves **a** Pure Pb:LT **b** Pb8Ni2:LT **c** Pb6Ni4:LT **d** Pb4Ni6:LT and **e** Pb2Ni8:LT

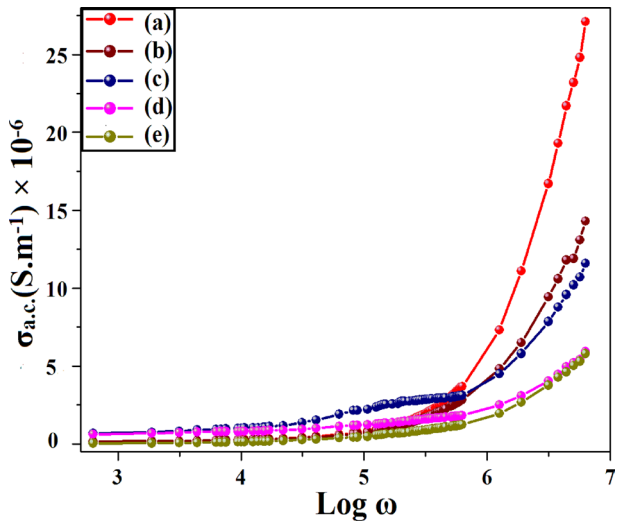

Fig. 9 The σ_{ac} versus angular frequency plots for **a** Pure Pb:LT **b** Pb8Ni2:LT **c** Pb6Ni4:LT **d** Pb4Ni6:LT and **e** Pb2Ni8:LT

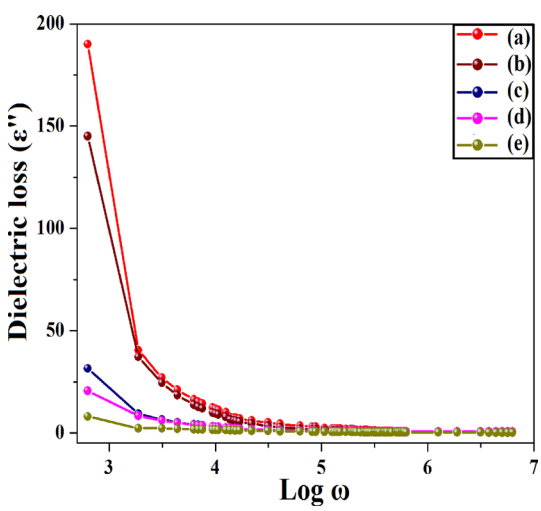

Fig. 8 Variation of (ε'') with angular frequency for **a** Pure Pb:LT **b** Pb8Ni2:LT **c** Pb6Ni4:LT **d** Pb4Ni6:LT and **e** Pb2Ni8:LT

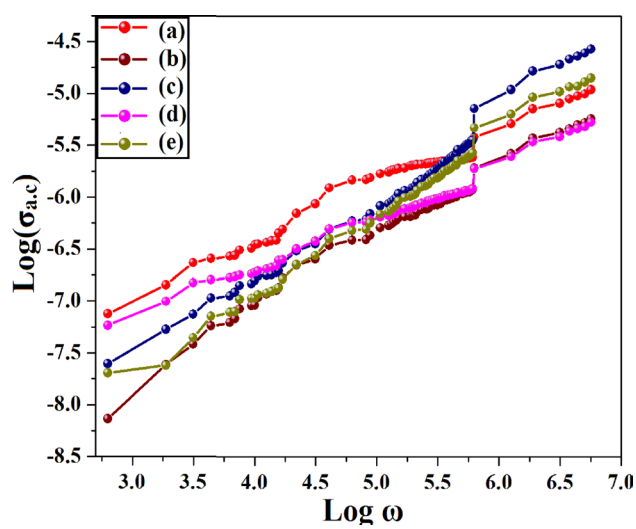

Fig. 10 Jonscher's curves for **a** Pure Pb:LT **b** Pb8Ni2:LT **c** Pb6Ni4:LT **d** Pb4Ni6:LT and **e** Pb2Ni8:LT

of molecules, i.e., higher polarizability of molecules is obtained for higher the dielectric constant of the material and vice versa. On this basis, similar trend of variation is observed for polarizability strength and dielectric constant of PbLT and Ni-added PbLT. The value of s in Jonscher's equation determines criteria of conduction mechanism [28–33].

The present study indicates the least exponent s values for PbLT, indicating the highest interaction of the mobile ions with lattice. The increase in the exponent s values is because of the Ni addition in PbLT indicating the decrement in interaction of the mobile ions with lattice around them as the presence of nickel occurs at grain positions. Further, a non-zero value of exponent s in the dispersive region of conductivity plot is attributed to the energy stored in the short-range collective motion of ions [34]. A higher value of s for nickel-added PbLT crystals implies that large energy is stored in such collective motions.

Table 10 Conductivity measurements for PbLT and Ni-added PbLT crystals

Sample no	DC conductivity ($\sigma_{dc}\times10^{-7}$) (S/m)	AC conductivity ($\sigma_{ac}\times10^{-5}$) (S/m)	s	$A\times10^{-9}$ (S m^{-1} rad^{-n})
(a) Pure Pb:LT	7.97	2.71	0.49	6.76
(b) Pb8Ni2:LT	1.54	1.43	0.53	4.74
(c) Pb6Ni4:LT	1.41	1.16	0.67	0.54
(d) Pb4Ni6:LT	0.56	0.59	0.80	0.31
(e) Pb2Ni8:LT	0.48	0.58	0.81	0.24

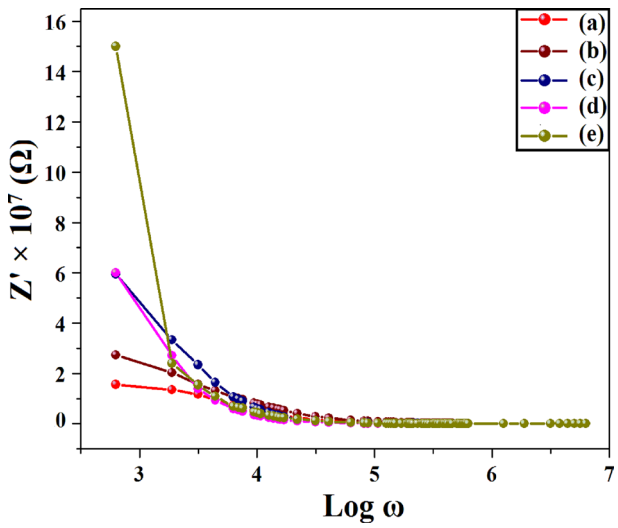

Fig.11 A plot of **a** Z' versus logω for **a** Pure Pb:LT **b** Pb8Ni2:LT **c** Pb6Ni4:LT **d** Pb4Ni6:LT and **e** Pb2Ni8:LT

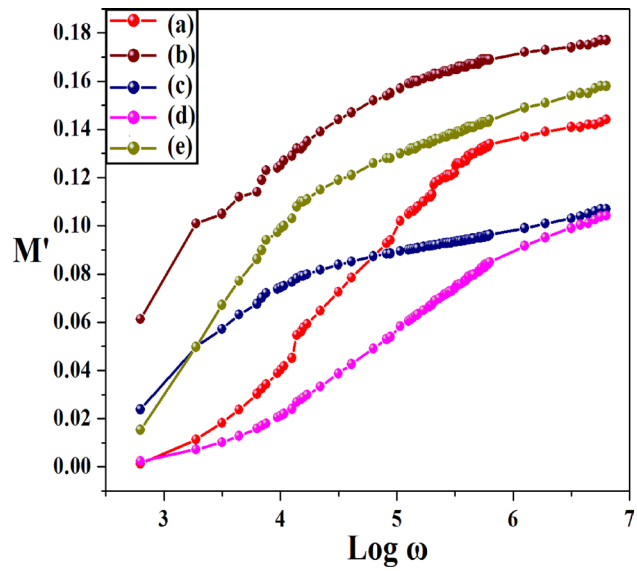

Fig. 12 A plot of M' versus logω for **a** Pure Pb:LT **b** Pb8Ni2:LT **c** Pb6Ni4:LT **d** Pb4Ni6:LT and **e** Pb2Ni8:LT

3.9 Impedance and modulus spectroscopic studies

Impedance and modulus spectroscopy are quite versatile to analyze various samples electrically and study their microstructural contributions [35–37]. The complex impedance and modulus study of PbLT and PbNiLT crystals were conducted at RT (room temperature) in the frequency interval 100 Hz to 1 MHz.

3.9.1 Z′ curves

Figure 11 depicts the plots of Z' real component of complex impedance (Z^*) versus angular frequency for Pb LT and PbNi LT crystals. All Z' curves exhibit same trend of variation for angular frequency, i.e., the Z' reduces in their values as the angular frequency increases and thereafter achieves almost a very low steady values and tends to merge together and becomes frequency independent.

The dispersion at low frequency regime is because of the occurrence of polarization and supports a slow dynamic relaxation taking place probably due to release of space charge at high frequencies [38]. This nature also correlated to the increase in AC conductivity with increase in frequency. The response of Z' at high frequency interval is due to the release of space charge [39]. Comparing the Z' curves, the PbLT shows the lowest value of Z' and correspondingly indicates the highest value of AC conductivity. As the Ni content (Wt%) increases in PbNiLT crystals, the value of Z' increases and correspondingly the AC conductivity decreases.

3.9.2 M′ curves

Figure 12 shows the plots of the real component of complex modulus (M^*) versus angular frequency for

PbLT and PbNiLT crystals. In the plots, the M' values are very small and approaches to zero indicating the removal of electrode polarization occurring [40, 41]. Further, the small value of M' in low frequency part is due to the shortage of restoring forces are prevailing [42], but with the conduction mechanism controlled by the long-range mobility of charge carriers [43].

The value of M' increases as the angular frequency increases and reaching to maximum value in high frequency part confirms the distribution of relaxation processes [44] and control of conduction mechanism by short-range mobile charge carriers [45]. The reason for dispersive nature of M' is because of spread of conductivity relaxation in different frequency ranges and further gives concurrence by the presence of loss peaks in the plots of imaginary part of electric modulus (M'') versus angular frequency. The M' plots of Fig. 12 show no peaks, which is due to the fact that the real component (M') of complex electrical modulus is equivalent to the real component of complex permittivity (ε'), i.e., M' represents the ability of the material to store the energy [46]. Very small values of M' for all the samples within lower frequency region result from the increase in the mobility of charge carriers.

3.9.3 Z'' curves

Figure 13 shows the plots of imaginary component (Z'') of complex impedance (Z^*) versus angular frequency for PbLT and PbNiLT crystals. In Fig. 13, the Z'' exhibits higher value in low frequency because of contributions of space charge polarization and its decrement is found at high frequencies [38].

The nature of Z'' curves indicates possibility of existence of a minor relaxation peak by moving to low frequency part in the case of PbLT crystals, which might be shifted toward further lower frequency side with increasing height with increase in concentration of nickel (Wt%) in PbLT crystals. However, this low angular frequency part where the peaks are expected to occur below the frequency range is used in the study. In the Z'' curve, the peak heights are showing proportionality to the bulk/grain resistance (R_g) [47]. The peak height increments of Z'' curves of PbNiLT in comparison to PbLT indicate increase in the impedance values and together the peak displacement to low angular frequency part implies the increase in the grain relaxation time τ_g. The Z'' curves become frequency independent and merge together in high angular frequency part as a reason of the space charge release in PbLT and PbNiLT crystals [39]. Further, the shift in relaxation peaks toward the origin, i.e., the lower frequency side, indicates a decrement in the rate of charge carrier hopping.

3.9.4 M'' curves

Figure 14 shows the graphs of imaginary component (M'') of complex modulus (M^*) versus angular frequency for PbLT and PbNiLT crystals. Figure 14

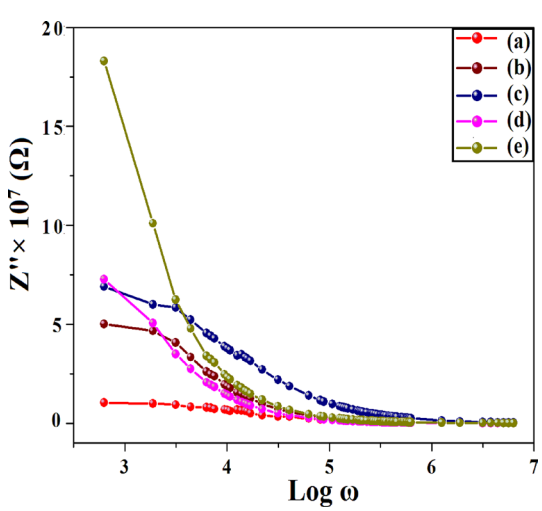

Fig. 13 A plot of Z'' versus logω for **a** Pure Pb:LT **b** Pb8Ni2:LT **c** Pb6Ni4:LT **d** Pb4Ni6:LT and **e** Pb2Ni8:LT

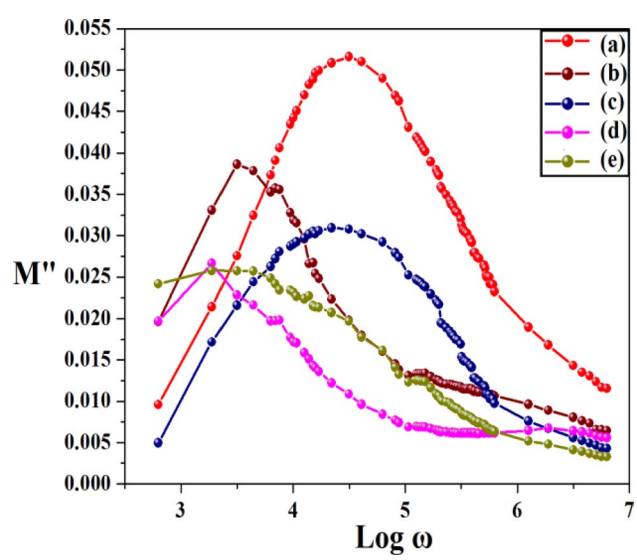

Fig. 14 A plot of M'' versus logω for **a** Pure Pb:LT **b** Pb8Ni2:LT **c** Pb6Ni4:LT **d** Pb4Ni6:LT and **e** Pb2Ni8:LT

depicts that M'' is very low, i.e., approaches to zero in the low frequency region, indicating the negligible electrode polarization [38]. The M'' curves acquire a single relaxation peak in the angular frequency region studied, implying that M'' curves represent the grain effect contribution only [39, 48]. The left-hand side part from the peak M'' gives the range where the charge carriers are delocalized and show the long ranged mobility, i.e., in other words doing successful hopping from one site to the other neighboring site. On the other hand, considering the region, right hand side of the peaks where the charge carriers are localized and confined to the potential wells prevailing and exhibit the short-range mobilities [41, 46, 58, 59].

The peak (M''_{max}) shifting toward low frequency side is due to Ni addition in Pb LT. This can be attributed to some variation in microstructure and cation distribution in the samples. Further, the irregular and asymmetric broadening of peaks indicates general distribution of relaxation time that specifies the existence of non-Debye type relaxation in the materials.

3.9.5 Complex modulus spectrum

The plots of M'' versus M', known as a complex modulus spectrum or as a Cole–Cole plots, indicate the mutual dependency of (M') and (M'') of complex modulus [42, 49] as shown in Fig. 15. The plots indicate single broad humps or arcs corresponding to single relaxation peaks over whole frequency range, suggesting the grain contributions in all the samples. The centers of these arcs or semicircles do not fall on the x-axis or the real axis suggesting the non-Debye type relaxation in all the samples and spread of relaxation. Figure 15 shows the lowest arc observed for Pb LT, indicating the highest grain capacitance of that sample.

By increasing content of Ni (Wt%) in Pb LT, the diameter or broadness of the arcs increases systematically, which consequently decreases the grain capacitance for these samples.

3.9.6 Complex impedance spectrum

The plots of Z'' versus Z', known as complex impedance spectra also known as Nyquist plots, show the mutual dependence of (Z') and (Z'') [42, 49]. The Nyquist curves of PbLT and Ni-added Pb LT are shown in Fig. 16. The curves are fitted with software Z view.

The formation of semicircular arc is obtained by extension of each curve bending toward real axis or X-axis. The formation of semicircles depends on strength of relaxation and frequency range [50, 51]. For all samples, the high frequency parts of arcs pass through the origins of the plots. The centers for each semicircle arcs are below the real axis, i.e., the depressed semicircles are found, which hint the prevalence of a non-Debye type of relaxation for all the samples. Total impedance of the polycrystalline material has contribution of grain, grain boundaries,

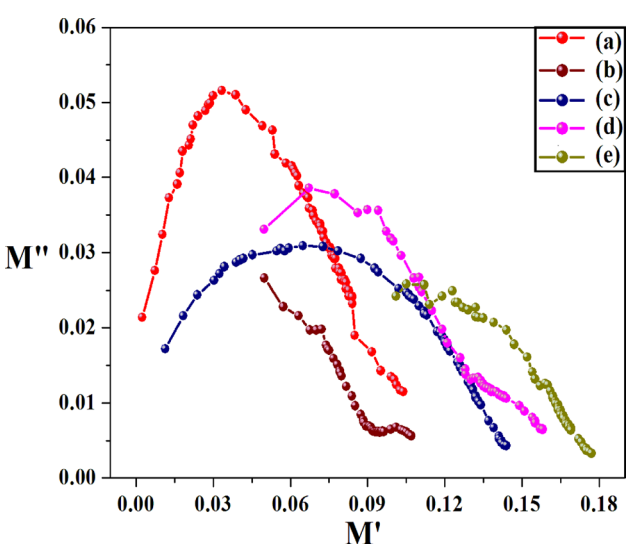

Fig. 15 Complex modulus spectrum for **a** Pure Pb:LT **b** Pb8Ni2:LT **c** Pb6Ni4:LT **d** Pb4Ni6:LT and **e** Pb2Ni8:LT

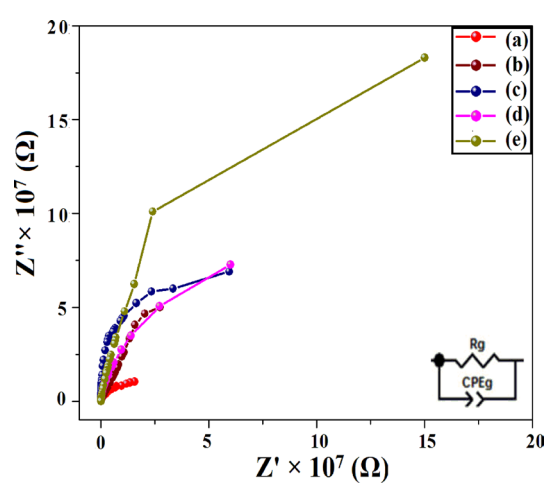

Fig. 16 Complex impedance spectrum for **a** Pure Pb:LT **b** Pb8Ni2:LT **c** Pb6Ni4:LT **d** Pb4Ni6:LT and **e** Pb2Ni8:LT

Table 11 Equivalent circuit parameters for the grown crystals

Sample Code	R_g(MΩ)	C_g (pF)	τ_g (ms)	α_g
(a) Pure Pb: LT	19	7.41	0.140	0.83635
(b) Pb8Ni2: LT	107	7.40	0.791	0.89215
(c) Pb6Ni4:LT	120	5.29	0.634	0.93739
(d) Pb4Ni6:LT	282	4.46	1.257	0.94933
(e) Pb2Ni8:LT	346	2.07	0.716	0.95028

and sample/electrode interface [52]. In the present case, single semicircular arcs are observed for Pb LT as well as Ni-added PbLT crystals over the whole frequency range under study indicating grain contribution to the total impedance of these crystals. The effect of Ni addition in PbLT is reflected by gradual increase in diameter of semicircular arcs indicating increase in grain resistance due to Ni addition in PbLT as mentioned in Table 11. The electrical modeling of microstructure is indicated by R-CPE parallel circuit as shown by inset Fig. in Fig. 16, which is fitted well with Nyquist curves indicating the correlation between electrical processes occurring within the material and microstructure.

In Fig. 16, the smallest semicircle is found for the PbLT crystals. As the content of Ni in PbNiLT increases, the diameter of the semicircular arc progressively increases. Such trends of variation in the diameters of Nyquist curves are indicating the increase in the values of grain resistance and, accordingly, reduction in the conductivity values of the crystals. The values of the grain resistance (R_g) and capacitance (C_g) are summarized in Table 11. The data are fitted with software Z view for equivalent circuit. Using Eq. (1), the relaxation times pertaining to grains were obtained.

$$\tau_g = R_g C_g \tag{1}$$

The amount of deviation from pure capacitor (α_g) for a grain can be calculated using standard equation which is given elsewhere [39]. The value of α_g is unity in the case of pure capacitor and it is zero for pure resistor.

Table 11 indicates lowest grain relaxation time in PbLT. As the concentration of nickel (Wt%) is increased in PbLT, the grain relaxation time increases, which shows that the presence of nickel raises the relaxation process of grain present in the samples. Further, the values of α_g increase by increasing Ni concentration in PbLT. This indicates that the system moves toward the ideal capacitive behavior.

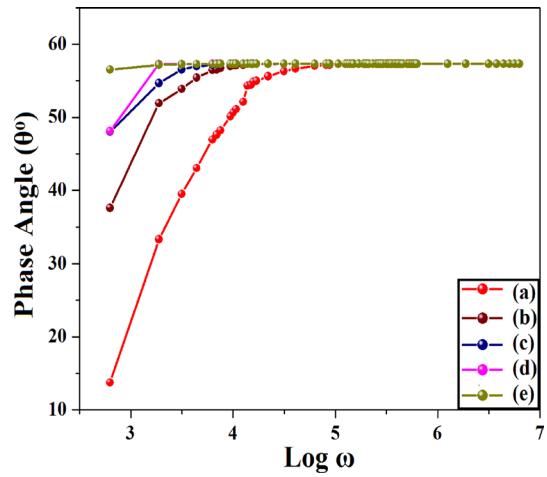

Fig. 17 Bode plot **a** Pure Pb:LT **b** Pb8Ni2:LT (**c**) Pb6Ni4:LT **d** Pb4Ni6:LT and **e** Pb2Ni8:LT

To recognize the relaxation process, present within all the samples clearly, the Bode plot is considered. Bode plots for all the samples are presented in Fig. 17.

The plots of phase of impedance versus angular frequency show that at lower frequencies the plots fall apart and at higher frequencies they merge together and hence the observed behaviors confirm the contributions from the grains only and the relaxation mechanisms can be shown by the equivalent parallel R-CPE circuits [39].

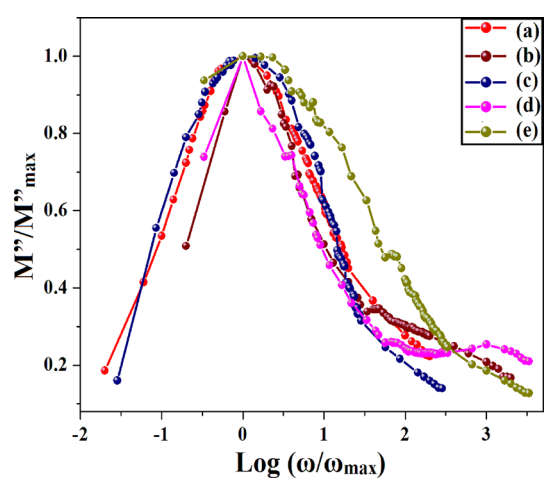

Fig. 18 Scaling of M″ for **a** Pure Pb:LT **b** Pb8Ni2:LT **c** Pb6Ni4:LT **d** Pb4Ni6:LT and **e** Pb2Ni8:LT

3.9.7 Scaling behavior of M″

To achieve the further information about the dependence of the relaxation dynamics on various factors such as temperature, structure, and the concentration of the charge carriers, the scaling behavior of M'' can be studied [46, 53]. The scaled M'' at room temperature is plotted against scaled angular frequency ω for PbLT and PbNiLT crystals as shown in Fig. 18. The M''_{max} and ω_{max} are employed as the scaling parameters for M'' and ω. As found from Fig. 18 and Fig. 14 that all modulus spectra for all the samples are overlapping but fail to merge in a single master curve, i.e., remains clear enough to be recognized. As the present investigation deals the effect of Ni addition on modulus properties PbNiLT crystals at room temperature, these results indicate that the relaxation dynamics occurring within the samples are dependent on the concentration of the charge carriers and that varies as per the Wt% of nickel in PbNiLT crystals.

The asymmetrical shapes of the plots indicate the deviation of dielectric relaxation process from the pure Debye behavior and existence of distribution of relaxation times. The non-symmetric normalized modulus plot corresponds to the non-exponential nature of the electrical function, which is described by the Kohlrausch-William-Watts exponential function [46, 53, 54] for the evaluation of exponential parameter (β). Presently, the FWHM (full width at half maximum) of M'' versus logω plots is found by applying Gaussian type curve fitting. The evaluated values of parameter β for grain relaxation are compiled in Table 12.

The $\beta = 1$ suggests Debye type relaxation, but as the β becomes smaller the higher is the deviation from Debye type relaxation. Presently, the value of β for pure crystal of PbLT is near to 1 and as the Wt% of Ni is increased in PbLT, the β moves away from one, indicating increase in deviation from Debye type relaxation.

There are several studies carried out using impedance spectroscopy on various materials in terms of effect of temperature on magnetite nano-particles to understand metal–semiconductor and semiconductor–metal transitions [55]; effect of dopant in KDP crystals [56]; role of doping in $Sr_{2-x}Ca_xNiWO_6$ [57]; effect of doping in CoS_2 thin films [58]; lead–cobalt levo-tartrate crystals [59]; and effect of Cu and Cr doping in barium hexa-ferrite [60]. The present work describes the effect of Ni addition on impedance properties clearly in lead levo-tartrate (PbLT) crystals. The AC electrical properties are important to explore to find its applications.

Table 12 Exponent parameter (β) values for PbLT and PbNiLT crystals

Sample Code	β value
(a) Pure Pb: LT	0.913
(b) Pb8Ni2: LT	0.805
(c) Pb6Ni4:LT	0.697
(d) Pb4Ni6:LT	0.665
(e) Pb2Ni8:LT	0.432

4 Conclusions

Dendrite crystals for pure Pb LT and Ni-added PbLT, i.e., PbNiLT were harvested by the single diffusion gel growth method. Dendrite and white PbLT were observed throughout the gel, starting from the gel–liquid interface. Dendrite-type crystals with changing density and coloration were obtained for PbNiLT crystals which depended on the volume concentration of the content lead and nickel. The elemental analysis confirmed major participation of Pb compared to Ni in compound formation due to its smaller hydrated radius. Powder XRD study confirmed that pure PbLT and PbNiLT crystals exhibited orthorhombic system and single phase in nature. The value of strain and crystallite size were calculated and reported. From FTIR spectra of pure PbLT and PbNiLT crystals, the C=O, C–H, C–O functional groups presence and water of hydration, and metal–oxygen group were confirmed. From the thermo-grams, it was noted that the crystals are decomposed by three stages, namely, anhydrous, carbonate, and oxide. Further, Ni addition slightly increased thermal stability of PbLT. Various AC electrical properties were studied in detail with variation of angular frequency. The dielectric investigations revealed classical dielectric behavior. The value of dielectric constant decreased in higher frequency regime. The nature of dielectric loss curve was in accordance with dielectric constant curves. The Ni addition in Pb LT reduced its dielectric constant and consequently its grain capacitance Cg. The decrement in grain capacitance C_g due to nickel at grain positions reduced the dielectric loss of Ni-added Pb LT crystals. The AC conductivity values increased with frequency and indicated decrease in AC conductivity due to increased grain resistance on Ni addition in PbLT crystals. The Jonscher's power law obeyed PbLT

and PbNiLT crystals. The values of s increased and A decreased on increasing Ni content in crystals suggested decrement of mobile ions with lattice surrounding as well as decrement in strength of polarizability. The Z' curves indicated increase in grain resistance, i.e., decrease in AC conductivity due to Ni addition in PbLT crystals. The M' curves indicated small M' values in the low frequency region and continuous dispersion and then almost constant values of M' in the high frequency part regarding all samples. The nature of Z'' curves indicated the increment in the peak height and its shifting toward lower frequency region on adding Ni in Pb LT crystals. The M'' curves indicated a single peak for PbLT and PbNiLT crystals. The low frequency shift in peak position was also observed in PbNiLT compared to pure PbLT indicating increase in the grain relaxation time. The complex modulus plane plot showed single semicircle for PbLT and PbNiLT crystals, indicating the grain contributions in samples. The trend of the complex impedance plane plot showed a bending toward real axis in all samples and suggested the existence of grain relaxation only within the frequency range studied. The same was modeled using R-CPE parallel circuit. As the Ni addition increased, the grain resistance increased and the grain capacitance decreased. The Bode plot confirmed the grain contribution and relaxation mechanisms given by the equivalent R-CPE circuit. The scaling behavior of M'' for all the samples showed overlapped modulus spectra for all the samples and remained clear enough to be recognized which indicates dependence of relaxation on concentration of impurity i.e., Wt% of Ni. The deviation of parameter β from unity indicated the existence of non-Debye-type relaxation samples. It is emphasized that the grain resistance (R_g), grain capacitance (C_g), and the stretch or deviation parameter β varied systematically with increase in Ni content in the crystals.

Acknowledgements

The author (NDP) acknowledges the encouragements from authority of Atmiya University, Rajkot and for providing the seed money. The authors are thankful to Librarian, Atmiya University, for providing software-based assistance. The authors are thankful to HOD, Physics, Saurashtra University, Rajkot for providing experimental facilities. One of the authors (JHJ) is highly thankful to Deputy Director, Regional Forensic Science Laboratory, Rajkot and the other author (RRH) is highly thankful to Director, FSL, Gandhinagar for allowing him to carry out such research activity.

Author contributions

NDP contributed toward data analysis & interpretation and writing, JHJ contributed toward technical contribution and revision, DJD contributed toward resource, RRH contributed toward resource, HOJ contributed toward review, writing & editing, and MJJ contributed toward review, writing & editing.

Funding

This research work is financially assisted by seed money project grant sanctioned by Atmiya University, Rajkot with S.L. No. SL/SMFAP/Phase 3/2023/006 dated on 10/07/2023.

Data availability

The research data of this manuscript will be made available on request.

Declarations

Conflict of interests The authors declare that they have no known competing financial interests or personal relationships that could have appeared to influence the work reported in this paper.

Supplementary Information The online version contains supplementary material available at https://doi.org/10.1007/s10854-024-12940-7.

References

1. N.J. Rahway, *The Merck Index of Chemicals and Drugs*, 6th edn. (Merck, 1952)
2. E. Coronado, J. R. Galan-Mascaros, L. J. Gomez-Garcia, A. Murcia-Martinez, Chem : A Eur. J. **12**(13), 3484 (2006). https://doi.org/10.1002/chem.200501351

3. Zhao, F., Zhang, H., Pei, Q., Gao, H., Zhang, X., Yi, J., Xu, S., Wang, J., Hao, H., Chen, X., Chinese patent : CN 101531587(2009)
4. H.K. Henisch, *Crystal growth in gels* (Pennsylvania Univ Press, 1970)
5. A.R. Patel, A.V. Rao, Bull. Mater. Sci. **4**, 527 (1982)
6. H.O. Jethva, M.J. Joshi, Bulg. J. Phys. **45**, 275 (2018)
7. H.O. Jethva, M.V. Parsania, Asian J. Chem. **22**(8), 6317–6320 (2010)
8. M. Abdulkadhar, M.A. Ittyachen, J. Cryst. Growth **39**(2), 365–366 (1977)
9. H.O. Jethva, P.M. Vyas, K.P. Tank, M.J. Joshi, J. Therm. Anal. Calorim. **117**(2), 589–594 (2014)
10. P.A. Savale, S.K. Bachhav, V.B. Suryawanshi, Int. J. Basic Appl. Res. **9**(2), 168–175 (2019)
11. P.W. Lau, W.C. Lin, J. Chem. Phys. **59**, 3981 (1973)
12. N. Satyanarayana, K. Hariharan, S. Radhakrishna, Physica B+C **122**(1), 67–73 (1983)
13. F. Jesu Rethinam, D. Arivu Oli, S. Ramasamy, P. Ramasamy, Cryst. Res. Technol. **28**, 861–865 (1993)
14. Q. Gao, Y.B. Xie, D. Wang, J. Chem. Crystall. **38**(8), 587–590 (2008)
15. A. Hoek, W.M.H. Sachtler, J. Catal. **58**, 276 (1979)
16. SGS Digicomply, Restricted Substances Data Base: Nickel Tartrate, Dec 16, 2022. https://www.digicomply.com/restricted-substances-mrl
17. Wired Chemist, Metallic, Covalent and Ionic Radii(r) data, http://www.wiredchemist.com/chemistry/data/metallic-radii
18. P.M. Dove, C.J. Nix, Geochim. Cosmochim. Acta **61**, 3331 (1997)
19. C.F. Albert, G. Wilkinson, P.L. Gaus, *Basic Inorganic Chemistry*, 3rd edn. (Wiley, 1995), p.292
20. G.K. Williamson, W.H. Hall, Acta Metall. **1**, 22–31 (1953)
21. John Coats 2000, Interpretation of Infrared Spectra, A Practical Approach, Ed. R. A. Meyers, Wiley, Chichester pp. 10815-10837
22. V. Mathivanan, M. Haris, T. Prasanyaa, M. Amgalan, Pramana-J. Phys. **82**(3), 537 (2014)
23. S. Ariponnammal, T. Srinivasan, Res J Recent Sci **3**, 63 (2014)
24. R.M. Silverstein, F.X. Webster, D.J. Kiemle, D.L. Bryce, *Spectrometric Identification of Organic Compounds*, 8th edn. (Wiley India Pvt. Ltd., New Delhi, 2019)
25. V.S. Joshi, M.J. Joshi, Indian J. Phys. **75**, 159 (2001)
26. J.C. Anderson, *Dielectrics* (Chapman and Hall, London, 1964), p.16
27. A.K. Jonscher, Nature **267**, 673–679 (1977)
28. B.H. Bhat, R. Samad, B. Want, Appl. Phys. A **122**, 1–11 (2016)
29. C. Karthik, K.B.R. Varma, J. Phys. Chem. Solids **67**, 2437 (2006)
30. K.L. Ngai, A.K. Jonscher, C.T. White, Nature **277**, 185 (1979)
31. A. Radon, D. Lukowiec, M. Kremzer, J. Mikula, P. Wlodarczyk, Materials **11**, 735 (2018)
32. K. Funke, Prog. Solid State Chem. **22**, 111 (1993)
33. K.A. Mauritz, Macromolecules **22**, 4483 (1989)
34. A.K. Jonscher, *Dielectric relaxation in solids* (Chelsa Dielectric Press, London, 1983)
35. M.J. Joshi, Mech. Mater. Sci. Eng. (2017). https://doi.org/10.2412/mmse.42.57.345
36. D.C. Sinclair, Bol. Soc. Esp. Cerám. Vidrio. **34**(2), 55–65 (1995)
37. J.R. Macdonald, *Impedance Spectroscopy: Theory, Experiment, and Applications* (Wiley, 2005)
38. R. Ranjan, N. Kumar, B. Behera, R.N.P. Choudhary, Adv. Lett. Mat. (2014). https://doi.org/10.5185/amlett.2013.fdm.52
39. J.H. Joshi, G.M. Joshi, M.J. Joshi, H.O. Jethva, K.D. Parikh, New J. Chem. **42**, 17227 (2018)
40. F. Yakuphanoglu, Physica B **393**, 139 (2007)
41. A. Dutta, T.P. Sinha, P. Jena, S. Adak, J. Non-Cryst. Solids **354**, 3952–3957 (2008)
42. L. Thansanga, A. Shukla, N. Kumar, R.N. Choudhary, Phase Transit. **94**(1), 47 (2021)
43. S.R. Hasan, U. Prasad, N. Kumar, R. Rajan, R.N.P. Choudhary, IJLTEMAS. **4**, 51 (2015)
44. L.N. Patro, K. Hariharan, Mater. Chem. Phys. **116**, 81 (2009)
45. N.K. Mohanty, S.K. Satapathy, B. Behera, P. Nayak, R.N.P. Choudhary, J. Adv. Ceram. **1**, 221 (2012)
46. S.B. Aziz, Z.H.Z. Abidin, A.K. Arof, Express Polym Lett **4**(5), 300 (2010)
47. P. Das, B. Pati, B. Sutar, R. Choudhury, J. Mod. Phys. **3**(8), 870 (2012)
48. U. Ahmadu, S. Tomas, S.A. Jonah, A.O. Musa, N. Rabiu, Adv. Mat. Lett. **4**(3), 185 (2013)
49. P.S. Sahoo, A. Panigrahi, S.K. Patri, R.N.P. Choudhary, Mater Sci Poland **28**, 763 (2010)
50. R.J. Gerhardt, Phys. Chem. Solids **55**, 1491 (1994)
51. R. Ranjan, N. Kumar, B. Behera, R.N.P. Choudhary, Adv. Mat. Lett. **5**(3), 138 (2014)
52. D. Shyamala, R. Rathikha, K. Gomathi, Int. J. Pure Appl. Phys. **12**(1), 35 (2016)
53. A. Karmakar, S. Majumdar, S. Giri, Phys. Rev. B (2009). https://doi.org/10.1103/PhysRevB.79.201202
54. S. Bhattacharya, A. Gosh, Solid State Ionics **161**, 61 (2003)

55. A. Ur-Rehman, M. Atif, M. Younas, T. Rafique, H. Wahab, A. Ul-Hamid, N. Iqbal, Z. Ali, W. Khalid, M. Nadeem, RSC Adv. **12**, 12344 (2022)
56. J.H. Joshi, G.M. Joshi, M.J. Joshi, K.D. Parikh, Ionics **25**, 3223 (2019)
57. N.A.F.M. Saadon, N.I. Taib, C.W. Loy, Z. Mohamed, Sci. Rep. **13**, 1246 (2023)
58. B. Benrabah, A. Bouaza, A. Kadari, M.A. Maaref, Superlattice Microstruct. **50**, 591 (2011)
59. H. Jethva, D. Kanchan, M. Joshi, Intl. J. Innov. Res. Sci. Engng. Technol. **5**, 221 (2016)
60. A.A. Gor, N.M. Devashrayee, T. Gupta, C.C. Chauhan, R.B. Jotania, Mater Today Commun. **37**, 107214 (2023)